Electronic Supporting information for

Green Synthesis of Porphyrin-based Self-assembled Nanocubes for Augmented Sono-Photodynamic Inactivation of Bacteria: A Sustainable Approach Towards Advanced Antimicrobial Strategies

*Pradeep Singh Thakur[a,] and Muniappan Sankar,[a,b]**

[a]Centre for Nanotechnology, Indian Institute of Technology Roorkee, Roorkee-247667, India

[b]Department of Chemistry, Indian Institute of Technology Roorkee, Roorkee-247667, India

***Corresponding author:** E-mail: *m.sankar@cy.iitr.ac.in*; Tel: +91-1332-284753

Table of Contents

EXPERIMENTAL SECTION:

Chemicals And Materials

4-Pyridinecarboxaldehyde and pyrrole were purchased from HiMedia and Alfa Aesar, respectively and used as received. Dipotassium hydrogen orthophosphate (K_2HPO_4) and potassium dihydrogen orthophosphate (KH_2PO_4) were purchased from Qualigens, India and used for the preparation of phosphate buffer solution (PBS). N, N-Dimethylformamide (DMF) and Cetyl trimethyl ammonium bromide (CTAB) were purchased from Thomas Baker and HiMedia, respectively and used as received.

All solvents employed in the present study were of analytical grade and were distilled before use. Zinc(II) acetate dehydrate was purchased from Sigma-Aldrich and used as received. All other chemicals were of reagent grade and used as received. Ultrapure MiliQ water was used for all synthesis and other experiments. Ultra-high purity water (resistivity of 18.2 MΩ·cm) was produced by a Milli-Q system (Milli-Q, Millipore Corp.). Column chromatographic purification was performed using Silica gel (100-200 mesh) purchased from Thomas Baker, India and used as received. TLC analyses were performed on 0.2 mm Merck pre-coated silica gel 60 F254 aluminium chromatographic plates. The Gram-negative bacterial strain *E. coli* (DH5α) and Gram-positive bacterial strain *S. aureus* (MTCC 737) were procured from a microbial type cell culture (MTCC), CSIR-IMTECH, Chandigarh (India).

Instrumentation and Characterization

The absorption and emission spectra were recorded using SHIMADZU UV–vis spectrophotometer (UV-2600) and Hitachi F-4600 fluorescence spectrophotometer, respectively using a pair of quartz cells of 3.5 mL volume and 10 mm path length. MALDI-TOF mass spectra were recorded on a Bruker UltrafleXtreme-TN MALDI-TOF/TOF mass spectrometer using HABA (40-hydrox- yazobenzene-2-carboxylic acid) as a matrix. ^{1}H NMR

spectra were recorded on a Bruker AVANCE DPX-400 MHz spectrometer. The chemical shifts (d) are expressed in ppm with Me_4Si as an internal standard (d = 0 ppm) in the respective deuterated solvents. Fourier Transform Infrared (FT-IR) spectra were obtained on a Bruker Vector 22 FT-IR spectrophotometer using KBr pellets. The field emission scanning electron microscopy (FE-SEM) images and energy dispersive X-ray spectra (EDAX) were collected from an FE-SEM, Thermo Fisher Scientific Apreo S LoVac instrument coupled with an energy-dispersive X-ray detector (EDX) operating at an accelerating voltage of about 15–20 keV. The transmission electron microscopy (TEM) images and selected area electron diffraction (SAED) patterns were obtained from a TECNAI G2 20 S-TWIN (FEI Netherlands) microscope, operating at 200 keV. All the FESEM and TEM images were processed using ImageJ (NIH, http://rsb.info.nih.gov/ij) software. TEM grids were prepared by placing 10 µL of the nanoparticles (NPs) solution on a carbon-coated copper grid and drying at room temperature. Determination of the size distribution and average diameter of nanoparticles with respect to their hydro-dynamic sizes was performed via dynamic light scattering (DLS) measurements (Malvern Nano-ZS Zetasizer) at 25 °C with 90° detection angle. For this, a diluted colloidal solution of NPs (50 µL, diluted up to 1 mL) was prepared in MiliQ water.

SYNTHETIC PROCEDURES

General procedure for functionalized porphyrins

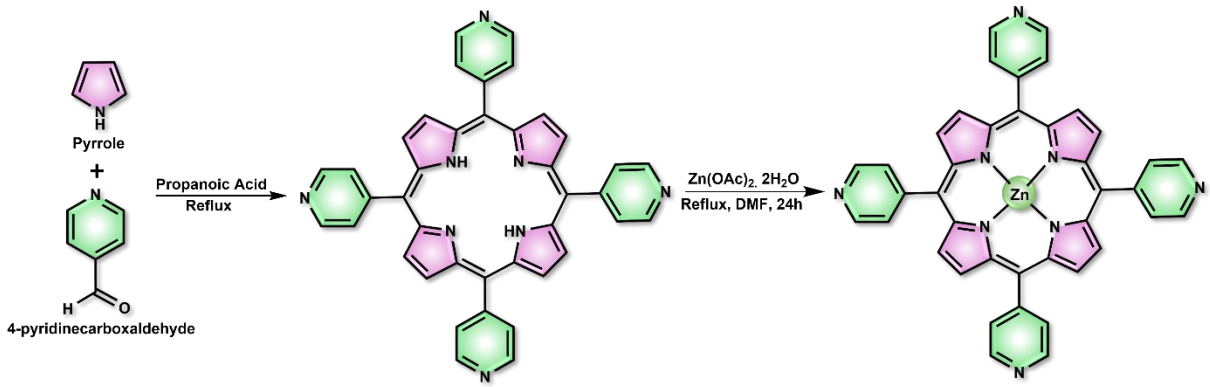

Scheme S1 Synthesis of H_2TPyP and ZnTPyP

Synthesis of *meso*-5,10,15,20-tetrakis(4-pyridyl)porphyrin [H_2TPyP] (1)

H_2TPyP (1) was prepared according to the modified Adler-Longo method.[1] In a typical reaction, 3.76 mL (0.04 mol) of 4-pyridinecarboxaldehyde and 2.8 mL (0.04 mol) of freshly distilled pyrrole were added to a round bottom (RB) flask containing 150 mL of propionic acid under reflux conditions. After completion of reaction, the reaction mixture was cooled to room temperature, distilled water (150 mL) was added to the reaction mixture and the product was extracted using 150 mL of dichloromethane. The pH of aqueous solution was in the range of 2.5–3.0. The crude product was purified by silica gel column chromatography using 5% methanol in chloroform as solvent eluent. After that violet purple solid was found as a pure product with 17% yield (115 mg, 0.101 mmol). UV-vis ($CHCl_3$): λ_{max} (nm): 417, 512, 546, 588, 646 . ^{1}H NMR (400 MHz, $CDCl_3$) δ (ppm): -2.93 (s, 2H, inner core N-H), 9.05-9.07 (dd, 8H, *β*-H), 8.87 (s, 8H, *o*-Ph-H), 8.15-8.17 (dd, 8H, *m*-Ph-H). MS (MALDI-TOF): calcd. 619.23 $[M+H]^+$, found 619.12.

Synthesis of *meso*-5,10,15,20-tetrakis(4-pyridyl)porphyrinato zinc (II) [ZnTPyP] (2)

150 mg (0.2426 mmol) of H_2TPyP was dissolved in a 10 mL of DMF. Then 798 mg (3.6 mmol) of $Zn(AcO)_2.2H_2O$, was added to the above solution, and refluxed for 48h. As the starting material was consumed (reaction monitored by UV−vis and TLC) the reaction mixture was cooled to room temperature and poured into water to obtain a solid. The solid was filtered off, washed with water 3 times to remove the excess of metal salt. The bright violet crystals were filtered off through G4 crucible and dried under vacuum. (Yield = 85%, 140 mg, 0.205 mmol). UV–vis ($CHCl_3$:MeOH (9:1, v/v)): λmax (nm): 425, 557, 597. ^{1}H NMR (400 MHz, $CDCl_3$/MeOD = 95/5) δ (ppm): 8.48 (s, 8H, *β*-H), 7.69 (s, 16H, *meso*-Ph-H). MS (MALDI-TOF): calcd. 680.141 $[M+H]^+$, found 680.068. All characterization data were consistent with the previous reports.[2]

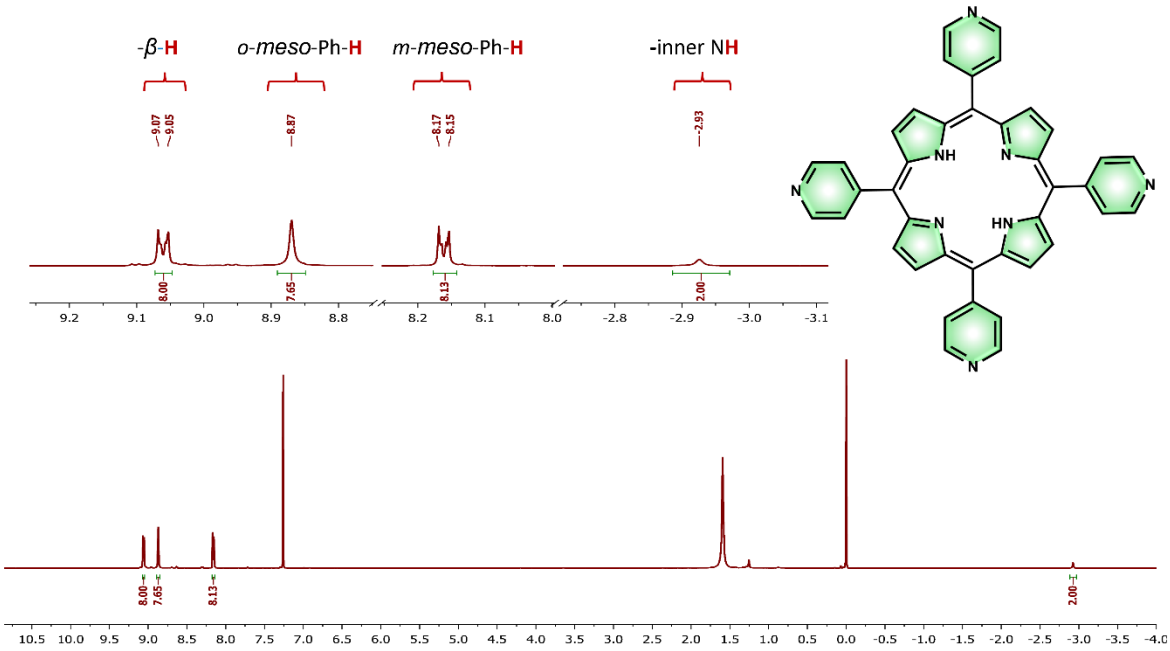

Fig. S1 ^{1}H NMR Spectrum of H_2TPyP in $CDCl_3$ at 298 K.

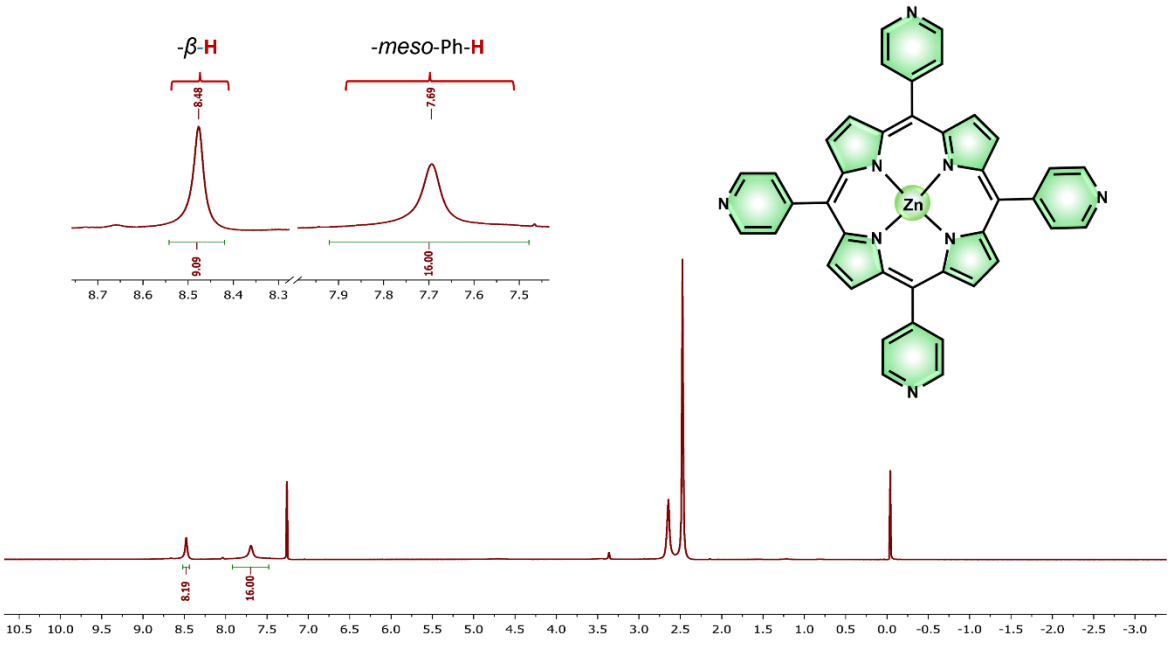

Fig. S2 ^{1}H NMR Spectrum of ZnTPyP in $CDCl_3$ at 298 K.

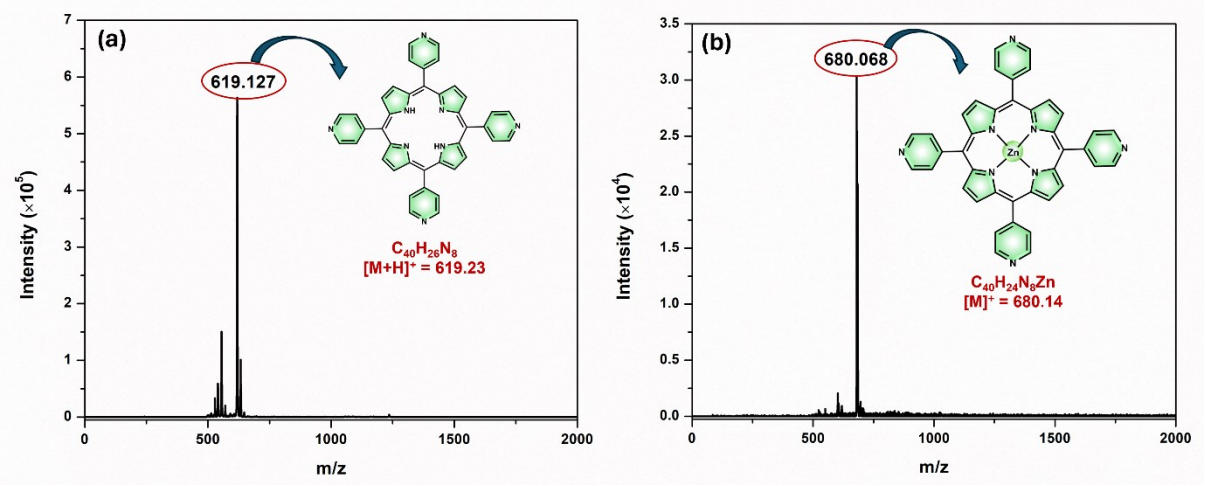

Fig. S3 MALDI-TOF mass spectrum of (a) H_2TPyP and (b) ZnTPyP in positive ion mode at 298 K.

Preparation of the green tea extract

To prepare green tea extract (GTE) for bio-inspired synthesis, green tea leaves (*Camellia sinensis*) powder of the Tetley brand, purchased from the local market, was used. This ready-to-use powder is already finely ground, allowing for efficient extraction of bioactive compounds. The brand was selected to ensure consistency and reproducibility, providing a reliable source of high-quality tea leaves with the desired phytochemicals.

The extraction is carried out using a Soxhlet apparatus. Weigh 50 grams of the powdered tea leaves and place them in a cellulose extraction thimble inside the Soxhlet extractor. Methanol, a highly polar solvent, is typically used for extraction due to its efficiency in extracting polyphenols, catechins, and other bioactive compounds. Add 200-300 mL of methanol to the Soxhlet's boiling flask. The solvent is then heated to its boiling point, causing it to vaporize, condense, and repeatedly wash over the green tea powder, ensuring thorough extraction. This process is usually maintained for about 24 hours.

After the extraction, the methanol containing the dissolved compounds is collected. The solvent is then removed using a rotary evaporator (rotavapor) under reduced pressure and at a low

temperature (40-50°C) to concentrate the extract. This method helps preserve the integrity of sensitive polyphenolic compounds, such as catechins. The concentrated extract is further dried in a vacuum oven at 40-50°C under reduced pressure until a dry powder is obtained. This dry GTE powder, which contains the bioactive compounds, is then stored in an airtight, amber-coloured container at 4°C to protect it from light, moisture, and degradation, ensuring its potency for future use.

When required for experiments, a specific amount of the GTE powder can be dissolved in deionized water to prepare an aqueous stock solution. This solution is then ready to be utilized in the bio-inspired synthesis of porphyrinic self-assembled nanoparticles, offering a green and sustainable approach to material synthesis.

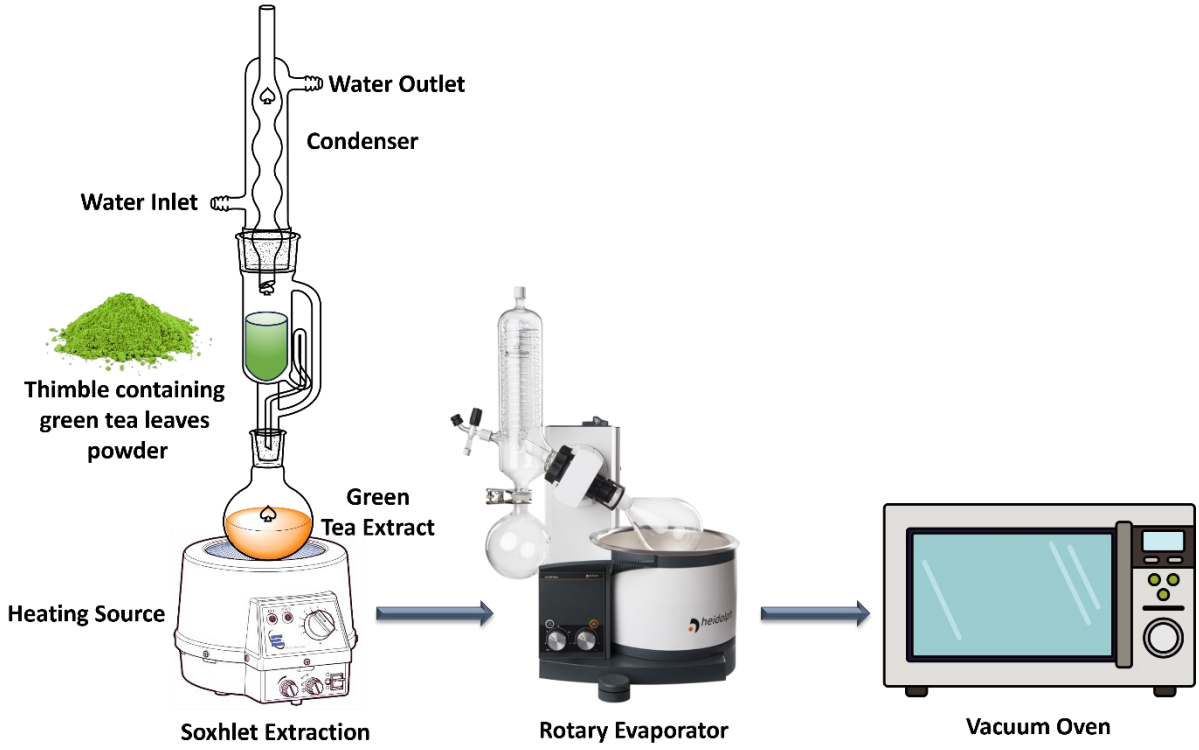

Scheme S2 General schematic for the preparation of green tea extract using Soxhlet extraction method.

General Procedure for Self-Assembled Nanoparticles

Chemical Synthesis of Zn(II)-tetrapyridylporphyrin Nanorods (CS-ZnTPyP-NRs)

In a typical preparation, 9.1 mL of aqueous solution containing cetyltrimethylammonium bromide (CTAB) (0.011 M) and NaOH (0.0027 M) was prepared at room temperature. Then we injected 0.45 mL of fresh stock ZnTPyP solution (0.01 M ZnTPyP dissolved in 0.05 M HCl solution) into it and stirred for 48 h. The final nanoparticles were collected by centrifugation at 12000 rpm and dried in vacuum oven.[3]

Green Synthesis of Zn(II)-tetrapyridylporphyrin Nanocubes (GS-ZnTPyP-NCs)

In a typical preparation, 9.1 mL of aqueous solution containing varied amounts of green tea extract (100µL, 200µL, and 300µL) from a 100 mg mL^{-1} of stock solution and NaOH (0.0027 M) was prepared at room temperature. Then we injected 0.45 mL of fresh stock ZnTPyP solution (0.01 M ZnTPyP dissolved in 0.05 M HCl solution) into it and stirred for 48 h. At every 6 h interval UV-vis spectra were taken for reaction optimization. The final nanoparticles were collected by centrifugation at 12000 rpm and dried in vacuum oven.

Characterizations

UV-vis spectroscopy

For UV-visible spectroscopy measurements, the spectra were recorded at room temperature. The choice of solvent and concentrations were optimized to ensure accurate and reproducible spectral data. The ZnTPyP was dissolved in a chloroform-methanol mixture (90:10) at a concentration of 1 mM. The green tea extract and the synthesized nanoparticles solution were prepared in water at a concentration of 100 µg mL^{-1}. These solutions were then analyzed to obtain their respective UV-vis spectra.

HPLC analysis of green tea extract

High-Performance Liquid Chromatography (HPLC) was conducted to confirm the presence of characteristic components of green tea extracts. A 500 µL sample of the green tea extract was taken and diluted with the appropriate solvent by adding the same volume to the volumetric vial. The sample vial was placed in the measuring apparatus, an HPLC SunFire-C18 column (5 µm, 4.6 mm × 250 mm; Waters Company). The mobile phase comprised solvents A (water with 0.1% formic acid) and B (acetonitrile/water = 80/20, v/v). The measurement was performed using a gradient elution: 5–40% of solvent B for 30 min with UV detection at a wavelength of 280 nm. The injection volume was 20 µL, and the flow rate was 1.0 mL/min.

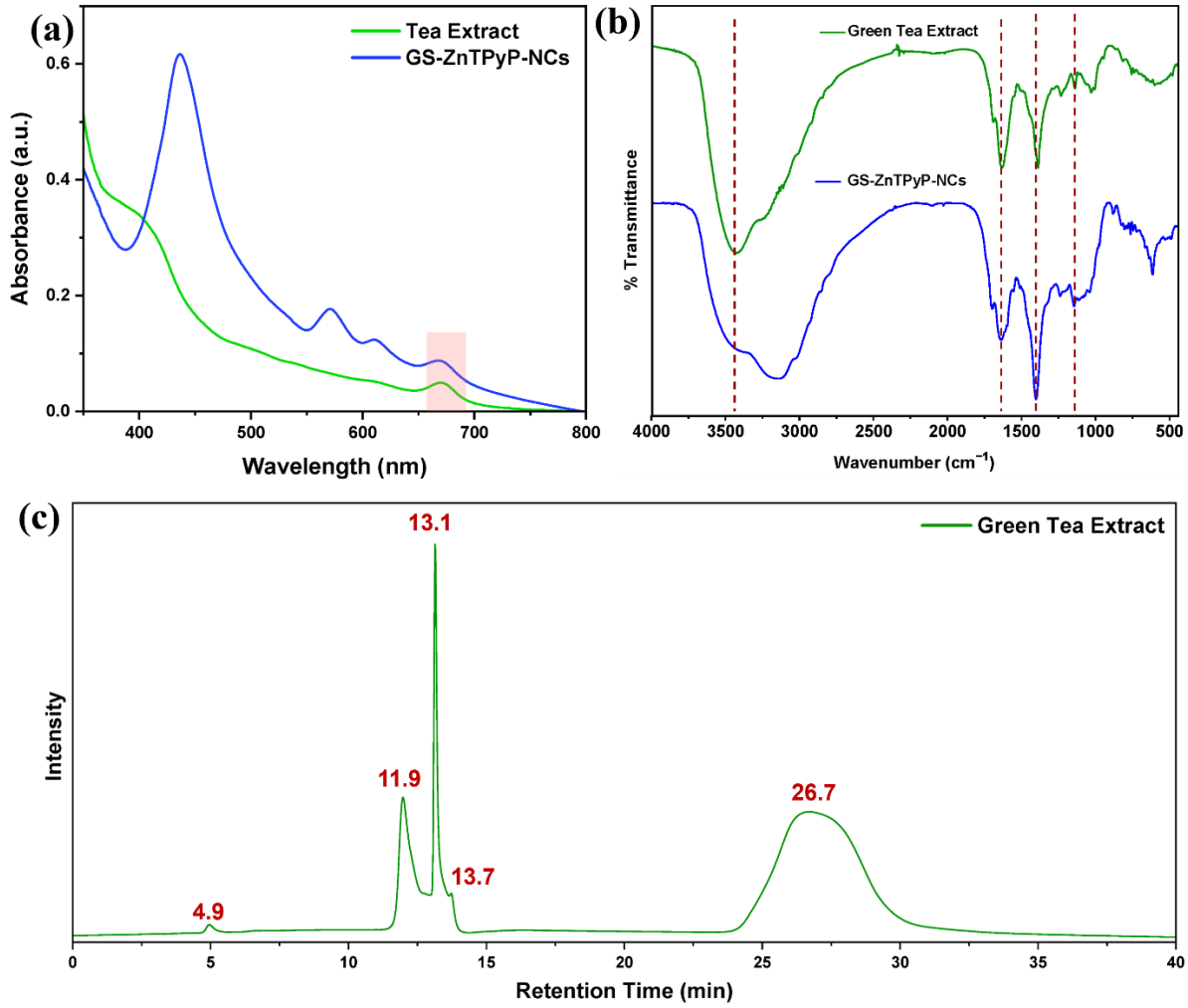

Fig. S4 Characterization of green tea extract and GS-ZnTPyP-NCs (a) UV-vis spectroscopy (b) FT-IR spectroscopy (c) HPLC chromatograph of green tea extract.

Table S1 HPLC analysis result of green tea extract (GTE).

Peak no.	Retention Time (min)	Peak Area	Peak Area%	Compound
1	4.953	141621	0.504	Galic acid (GA)
2	6.679	36709	0.131	Gallocatechin (GC)
3	11.972	3832628	13.637	Epigallocatechin (EGC)
4	13.140	3687104	13.119	Caffeine (CAF)
5	13.722	61542	0.219	Epicatechin (EC)
6	16.255	104702	0.373	Epigallocatechin gallate (EGCG)
7	16.478	63987	0.228	Catechin (C)
8	26.717	20006045	71.182	Epicatechin gallate (ECG)

Chemical structures of the compounds derived from green tea extract

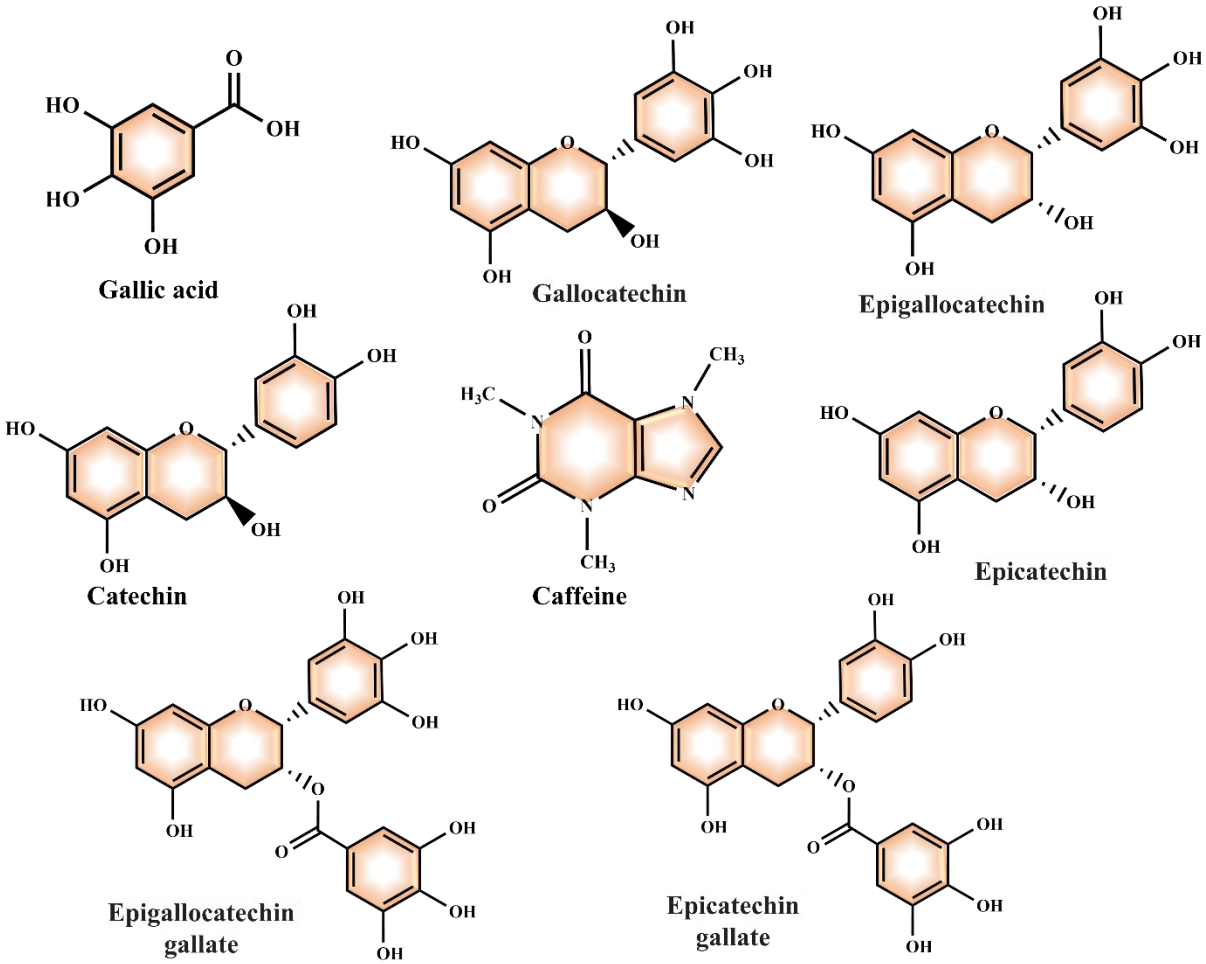

Fig. S5 The chemical structures of all the biomolecules identified through the study that attend the biosynthesis process: epicatechin and its derivatives, especially EGC, EGCG and ECG.

Table S2 FTIR analysis of green tea extract (GTE) and GS-ZnTPyP-NCs.

	Wavenumber (cm^{-1})	**Functional Group Assignment**
Green tea extract (GTE)	3450-3350	O–H stretching of polyphenols
	1638.53	C=O stretching of polyphenols and C=C stretching of aromatic compounds
	1394.87	C–H bending (methyl and methylene groups)
	1240.29	C–C stretching (associated with phenolic compounds)
	1146.43	C–O stretching (ethers, alcohols)
	1036.01	C–O stretching of polyphenolic compounds
	1011.31	C–H bending vibrations of aromatic compounds
GS-ZnTPyP-NCs	3358-3024	O–H stretching of polyphenols
	1640-1594	C=O stretching of polyphenols and C=C stretching of aromatic compounds and C=N stretching vibration of the *meso*-attached pyridyl substituents in ZnTPyP
	1401.83	C–H bending (methyl and methylene groups)
	1238.55	C–C stretching (associated with phenolic compounds)
	1144.49	C–O stretching (ethers, alcohols)
	1040.25	C–O stretching of polyphenolic compounds
	611.64	C=N bending vibration of ZnTPyP

Optimization of bio-inspired synthesis of ZnTPyP NCs through Dynamic Light Scattering (DLS) analysis and Field-Emission Scanning Electron Microscopy (FE-SEM) imaging

Table S3 Time-dependent values of hydrodynamic diameter (nm), zeta potential (mV), and polydispersity index (PDI) of Green Synthesized (GS)-ZnTPyP NCs*.

Composition	Time Interval (h)	Hydrodynamic diameter (nm)	PDI	Zeta potential (mV)
ZnTPyP (0.01 M) Tea Extract (0.05 mg mL^{-1})	0	1101.5 ± 84	0.214	−17.5
	6	650.6 ± 28	0.185	−18.3
	12	742.8± 35	0.245	−18.2
	18	683.0 ± 32	0.354	−20.8
	24	626.5± 28	0.387	−26.2
	48	675.8± 28	0.411	−24.9
ZnTPyP (0.01 M) Tea Extract (0.1 mg mL^{-1})	0	1503.1 ± 12.1	0.278	−17.5
	6	538.5± 28	0.318	−18.3
	12	240.6 ± 18	0.374	−18.4
	18	307.1 ± 19	0.278	−21.1
	24	339.9± 11	0.299	−26.2
	48	345.7± 14	0.317	−21.4
ZnTPyP (0.01 M) Tea Extract (0.15 mg mL^{-1})	0	1685 ± 78	0.317	−14.8
	6	711.5 ± 47	0.568	−14.2
	12	456 ± 38	0.891	−16.7
	18	657.8 ± 45	1.0	−18.8
	24	748 ± 58	1.0	−18.2
	48	2297.5 ± 87	1.0	−17.2

*All sampling procedures and measurements were carried out in triplicate, ensuring a total of three repetitions for each sample.

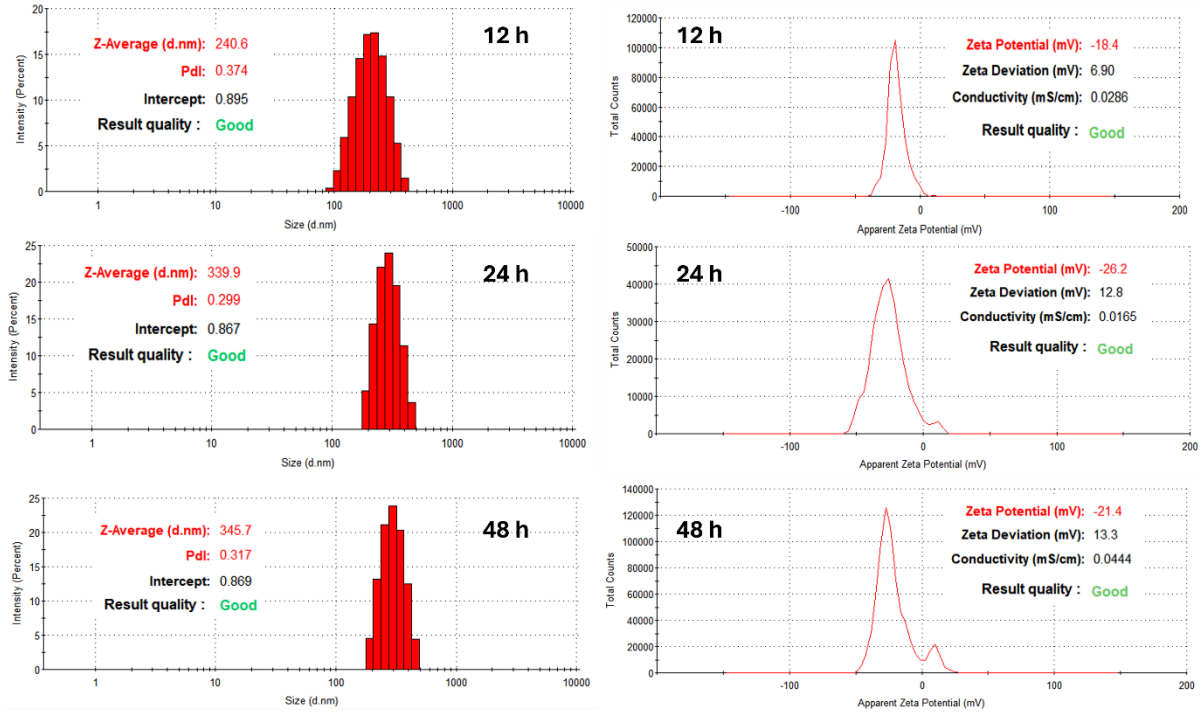

Fig. S6 Hydrodynamic diameter (nm), zeta potential (mV), and polydispersity index (PDI) of GS-ZnTPyP-NCs at 12 h, 24 h and 48 h (tea extract concentration 0.1 mg mL^{-1}).

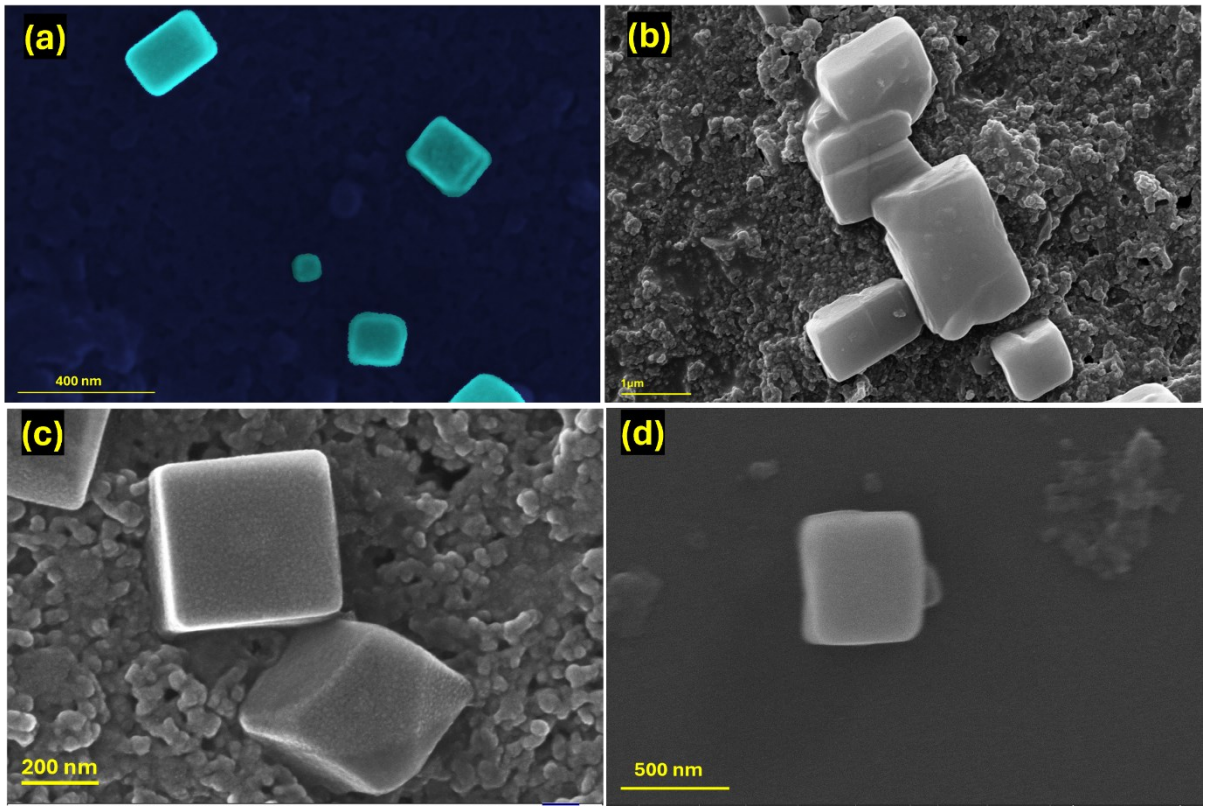

Fig. S7 FESEM micrograph of (a) GS-ZnTPyP-NCs. (b-d) time-dependent self-assembly of GS-ZnTPyP-NCs at (b) 6 h (c) 18 h, and (d) 24 h.

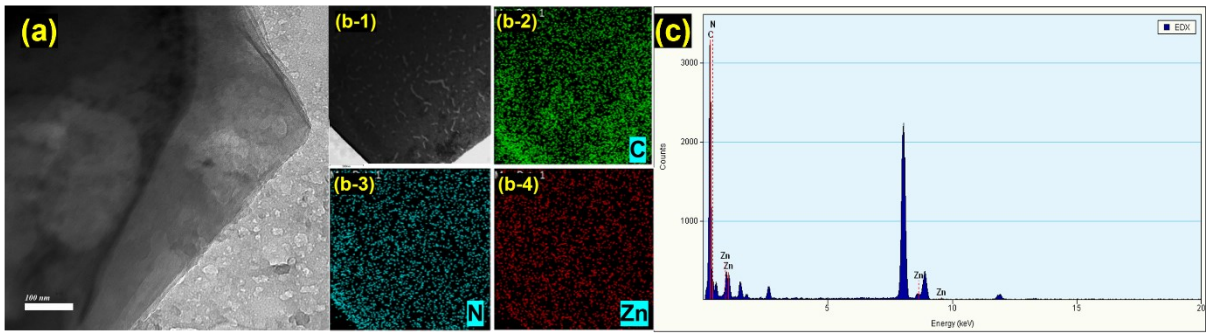

Fig. S8 (a) TEM image of GS-ZnTPyP-NCs, (b-1) Bright field STEM image and EDX element mapping of (b-2) C–K, (b-3) N–K and (b-4) Zn–K in GS-ZnTPyP-NCs, (c) EDX spectrum of GS-ZnTPyP-NCs.

Plausible mechanism of ZnTPyP nanocubes synthesis via bioinspired route

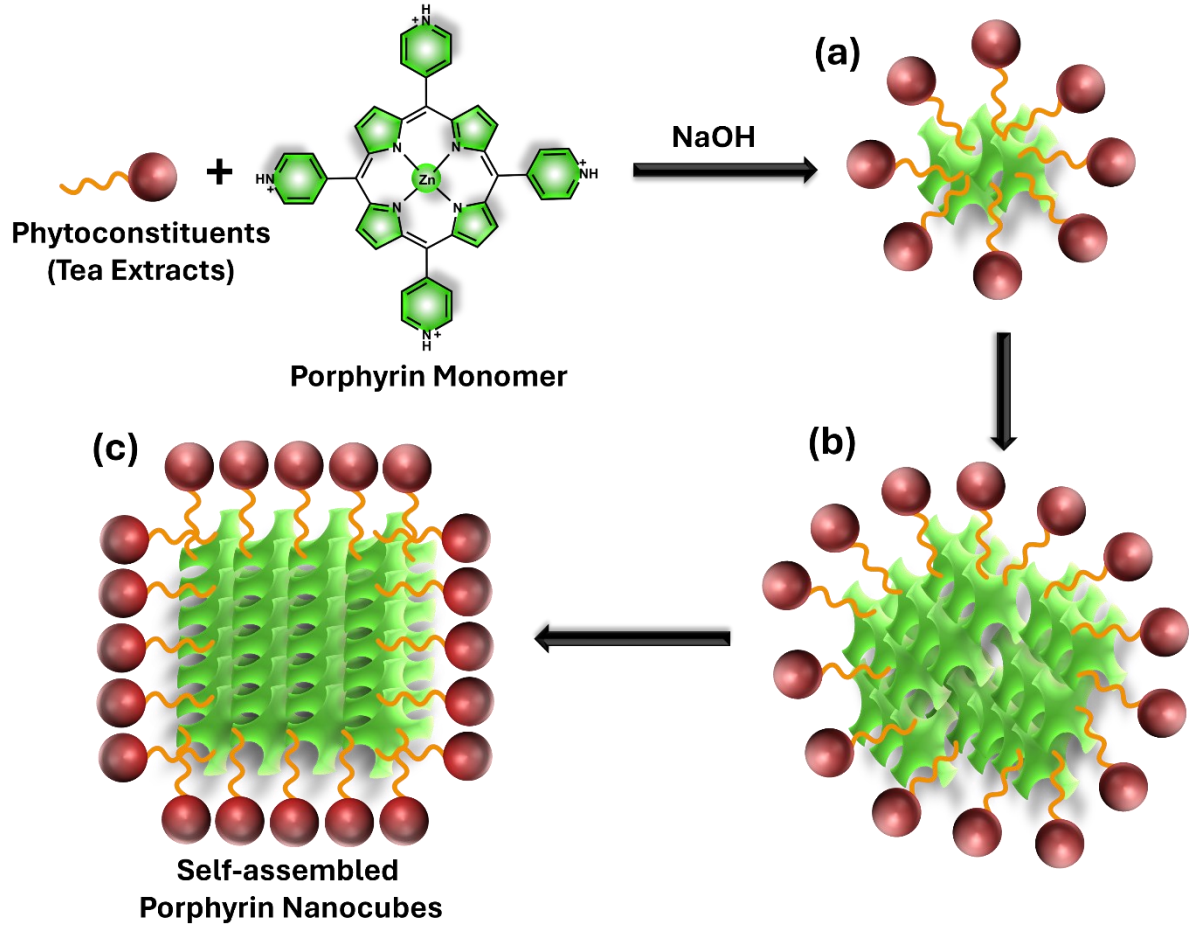

Fig. S9 Plausible Mechanism of Porphyrinic Nanocubes Synthesis via Bioinspired Route. (a) Encapsulation of porphyrin monomer (green-coloured) inside the phytoconstituents (catechins) micelle. (b) Nucleation of porphyrin aggregation within the micelle. (c) Growth of porphyrinic nanocubes.

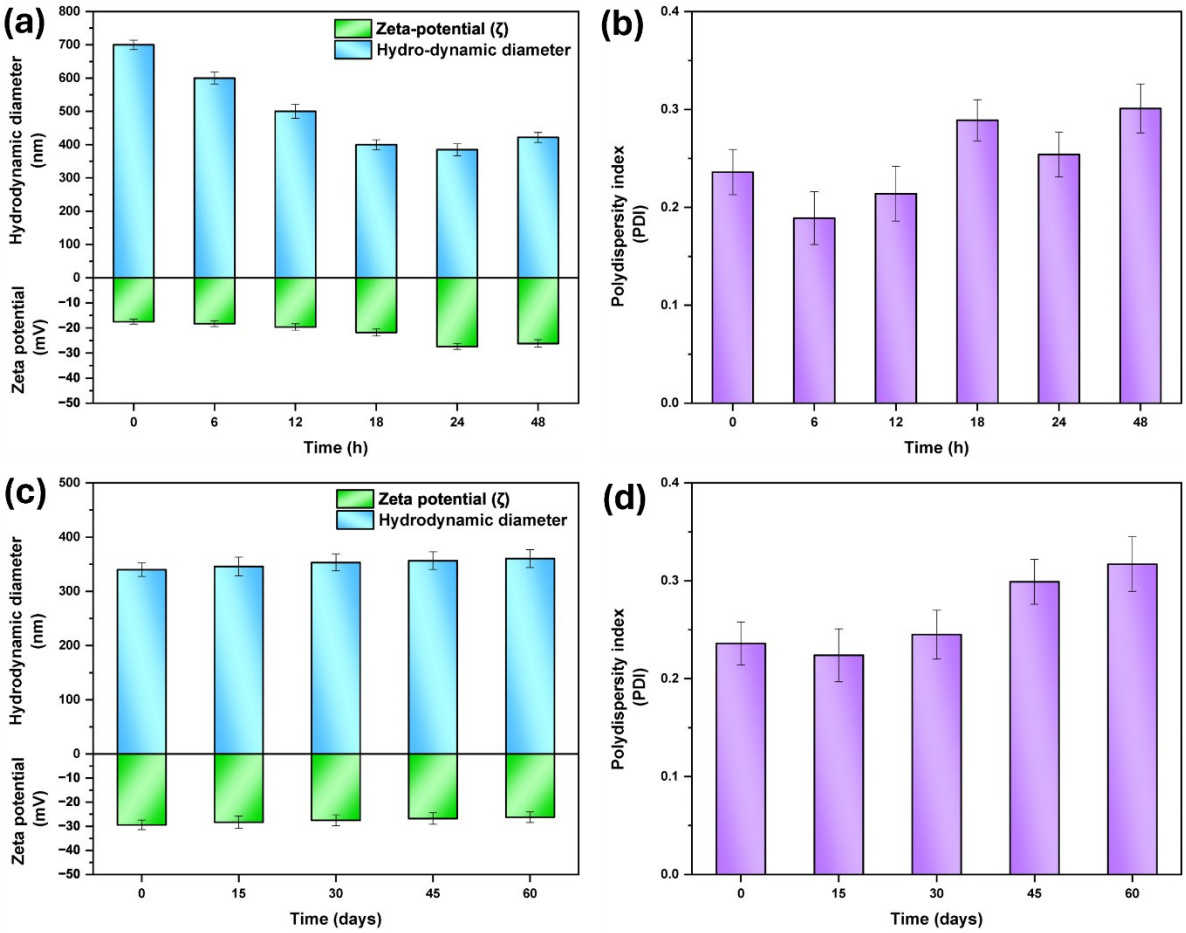

Fig. S10 Short and long-term storage stability of GS-ZnTPyP-NCs. (a) Hydrodynamic diameter, zeta potential, and (b) polydispersity index of GS-ZnTPyP-NCs at physiological conditions. (c) Hydrodynamic diameter, zeta potential, and (d) polydispersity index of GS-ZnTPyP-NCs upon long-term storage at 4 °C.

Determination of the Singlet Oxygen ($^1O_2$) Generation Efficiency

1,3-Diphenylisobenzofuran (DPBF) was chosen as an indicator of $^1O_2$ since this reactive oxygen species is able to trigger ring opening reaction of DPBF and thus cause decrease of absorbance at around 410 nm. By monitoring the absorbance of indicator during the irradiation time, $^1O_2$ generation efficiency of different photosensitizers can be reasonably compared according to the decrease rate of the absorbance. Because of the insolubility of DPBF in water, the reaction was performed in acetonitrile (CH_3CN) solution. Briefly, 100 µL of ZnTPyP NPs solution was mixed with DPBF solution (6×10^{-5} mol L^{-1} in acetonitrile, 900 µL), and the

resulting solution was adjusted to pH 7.4 . Then above solutions were irradiated with ultrasound (US) and 670 nm deep-red light LEDs separately and combined for different times (0 s, 30 s, 1 min, 1.5 min, 2 min, 3 min). Meanwhile, the absorption spectra of each solution were measured by UV-vis spectroscopy after irradiation. The blank and control groups were carried out with the parallel groups and irradiated under the same conditions.

Singlet oxygen quantum yield (SOQY) of TPP (**ΦΔ**; 0.64) was used as the standard reference and the slopes were deduced for the test and the standard. The SOQY was calculated by a comparative method using equation Eq. S1 and the mechanism involved in the cleavage of DPBF is depicted in scheme S2.

$$\boldsymbol{\Phi}_{\Delta_T} = \boldsymbol{\Phi}_{\Delta_S} \times \frac{m_T}{m_S} \times \frac{F_S}{F_T} \times \frac{\eta_T^2}{\eta_S^2} \quad \text{.....(Eq. S1)}$$

Here, m signifies the slope change in the absorbance of DPBF (at 411 nm) with the irradiation time, and F is the absorption correction factor, F = 1-10^{-OD}, where OD denotes optical density at the irradiation wavelength. The refractive index of the solvents is represented as η and subscripts 'T' and 'S' designate test and standard, respectively.

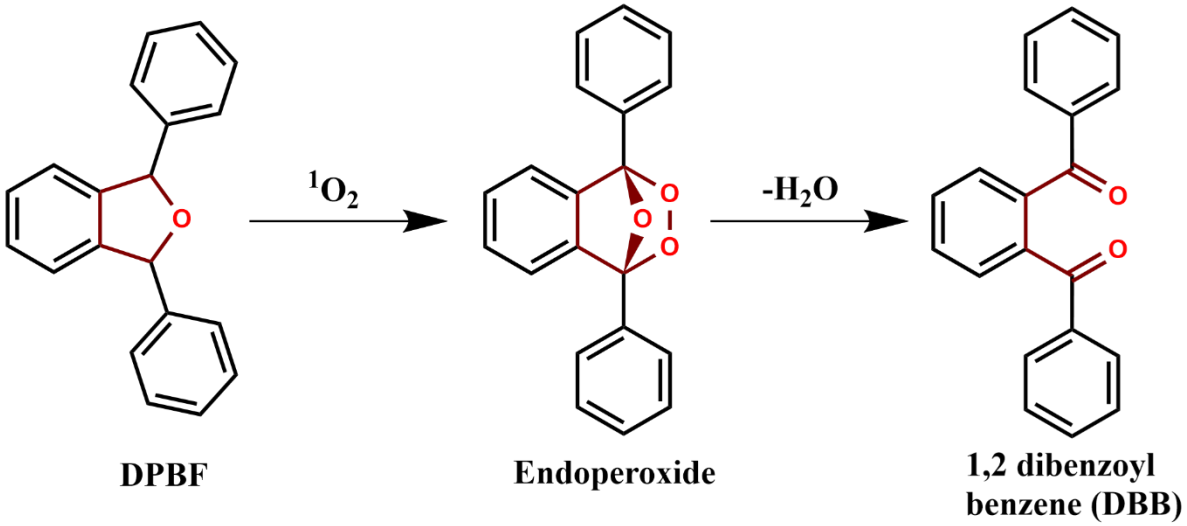

Scheme S3: Mechanism of DPBF degradation in the presence of singlet oxygen

Table S4. Singlet oxygen quantum yield (**ΦΔ**) of synthesized porphyrinic nanoparticles when irradiated with ultrasound (US), deep-red light (670 nm) LEDs, and dual mode (US and deep-red light)*

S. No.	Sample	Standard curve	ΦΔ
1	DPBF+ deep-red light (L)	y = -0.0015x + 1.200	0.01
2	DPBF+US	y = -0.0021x + 1.201	0.01
3	DPBF+ US + L	y = -0.0028x + 1.200	0.02
4	CS-ZnTPyP-NRs + DPBF + L	y = -0.0685x + 1.217	0.61
5	GS-ZnTPyP-NCs + DPBF + L	y = -0.0737x + 1.214	0.66
6	CS-ZnTPyP-NRs + DPBF + US	y = -0.0784x + 1.213	0.70
7	GS-ZnTPyP-NCs + DPBF + US	y = -0.0850x + 1.210	0.76
8	CS-ZnTPyP-NRs + DPBF + US+ L	y = -0.1095x + 1.209	0.98
9	GS-ZnTPyP-NCs + DPBF + US+ L	y = -0.1248x + 1.195	>0.99
10	GS-ZnTPyP-NCs + DPBF + US+ L+ NaN_3	y = -0.0044x + 1.201	0.03

Light doses (J cm^{-2}) calculations and dose of ultrasound:

In the study, deep red (670 nm) LEDs with a power output of 9 mW were positioned 10 cm above a 5 x 5 cm^2 surface area. Following the reported literature,[4] the light energy dose was calculated using the formula

$$E = Pt \quad \text{(Eq. S2)}$$

where E is the energy density (dose) in J cm^{-2}, P is the irradiance (power density) in W cm^{-2}, and t is the duration of treatment.[5]

Ultrasound (US) dose was given at a frequency of 1.0 MHz, and power density of 1.5 W cm^{-2} for the duration of 20 min.

Table S5. Light energy dose for sono-photo-responsive studies.

S. No.	Time (mins)	Light Energy Dose (J/cm^2)
1	5	1.8
2	10	3.6
3	15	5.4
4	20	7.2

Determination of Reactive Oxygen Species (ROS) generation ability

The ROS generation ability of ZnTPyP NPs were measured using UV-vis spectroscopy with 1,3-diphenylisobenzofuran (DPBF), methylene blue (MB), and nitroblue tetrazolium (NBT) as probes, under combined ultrasound (US) and light irradiations. DPBF was used to detect singlet oxygen ($^1O_2$), MB for hydroxyl radicals (•OH), and NBT for superoxide anion ($\bullet O_2^-$). Initially, solutions of each probe were prepared in appropriate solvents—DPBF in ethanol, and MB and NBT in water at suitable concentrations. ZnTPyP NPs were dispersed in a solvent to form a homogeneous suspension, which was then aliquoted into separate test tubes for each ROS detection method. The probe solutions were added to the corresponding test tubes, and the initial absorbance was measured using a UV-vis spectrophotometer at specific wavelengths: 410 nm for DPBF, 664 nm for MB, and 260 nm for NBT. The samples were then exposed to ultrasound (US) and simultaneously to light (670 nm) irradiation for different time intervals (0 s, 30 s, 60 s, 90 s, 120 s, 150 s and 180 s). Following the irradiation, the absorbance of each sample was measured again to determine the extent of ROS generation by comparing the post-irradiation absorbance values with the initial ones. Control experiments were conducted without NPs and without US and light irradiation to account for background ROS generation. The decrease in absorbance for DPBF, MB, and NBT after treatment indicated the production of $^1O_2$, •OH, and $\bullet O_2^-$ respectively, confirming the ROS generation capability of the ZnTPyP NPs under the experimental conditions.

Scavenging study

To verify that the reactive oxygen species (ROS), including, singlet oxygen ($^1O_2$), hydroxyl radical (•OH) and superoxide radical ($•O_2^-$) are formed under the sono-photodynamic therapy (SPDT) conditions, a scavenging study was conducted following the protocols reported in the literature.[6] Specific scavengers were used for each ROS, such as sodium azide was employed as the singlet oxygen ($^1O_2$) scavenger,[7] isopropanol (IPA) was used to scavenge hydroxyl radicals (•OH),[6] and *p*-benzoquinone (*p*-BQ) served as the scavenger for superoxide radicals ($•O_2^-$).[6] In this study, the ZnTPyP NPs were subjected to the same SPDT conditions in the presence of each scavenger, and the effect on the degradation of the respective probe for each ROS was monitored using UV-vis spectroscopy. By comparing the degradation rates of the probes with and without the presence of scavengers, the role of $^1O_2$, •OH, and $•O_2^-$ in the ROS generation process was confirmed. A significant reduction in probe degradation in the presence of the specific scavenger indicated the successful quenching of the corresponding ROS, thereby validating the formation of these reactive species during the SPDT treatment.

Electron spin resonance (ESR) measurements using spin trapping reagent

To further determine ROS types, the electron spin resonance (ESR) spectra were measured with 2,2,6,6-tetramethylpiperidine (TEMP) as a spin traps to capture singlet oxygen ($^1O_2$) and 5,5-dimethyl-1-pyrroline N-oxide (DMPO) as a trapping agent for hydroxyl (•OH) and superoxide radicals ($•O_2^-$) in deionized water and methanol, respectively. The 20 µL of spin trap agents and 50 µL solution of ZnTPyP nanoparticles (400 µg mL^{-1}) were mixed in capillary tubes and irradiated with combined US and light for 10 min. ESR assays were carried out at room temperature operating at 9.45 GHz of the microwave frequency, 15 mW of microwave power, 3100-3600 G of scanning field, 0.8 G of modulation amplitude, 15.5 S of the scan time, and 32 scan number.

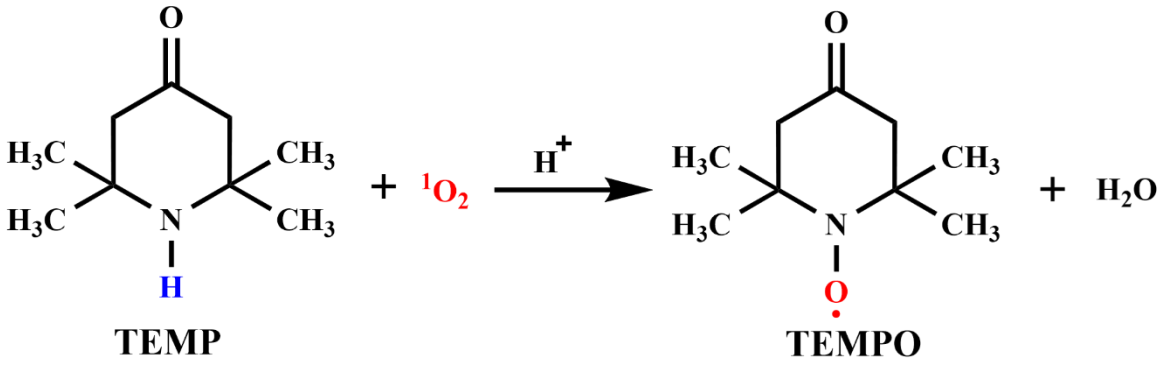

Scheme S4: Mechanism of TEMPO formation in the presence of singlet oxygen.

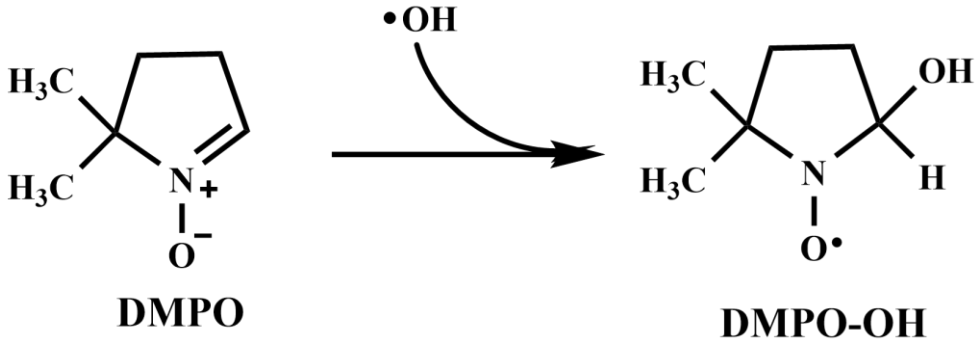

Scheme S5: Mechanism of DMPO-OH formation in the presence of hydroxyl radical.

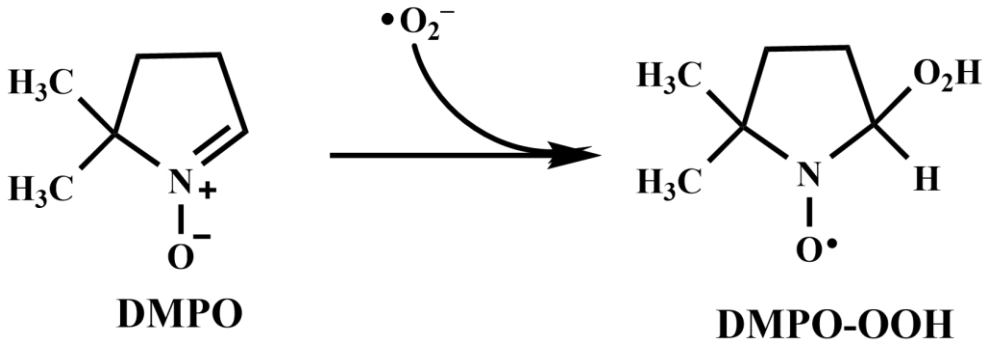

Scheme S6: Mechanism of DMPO-OOH formation in the presence of superoxide radical.

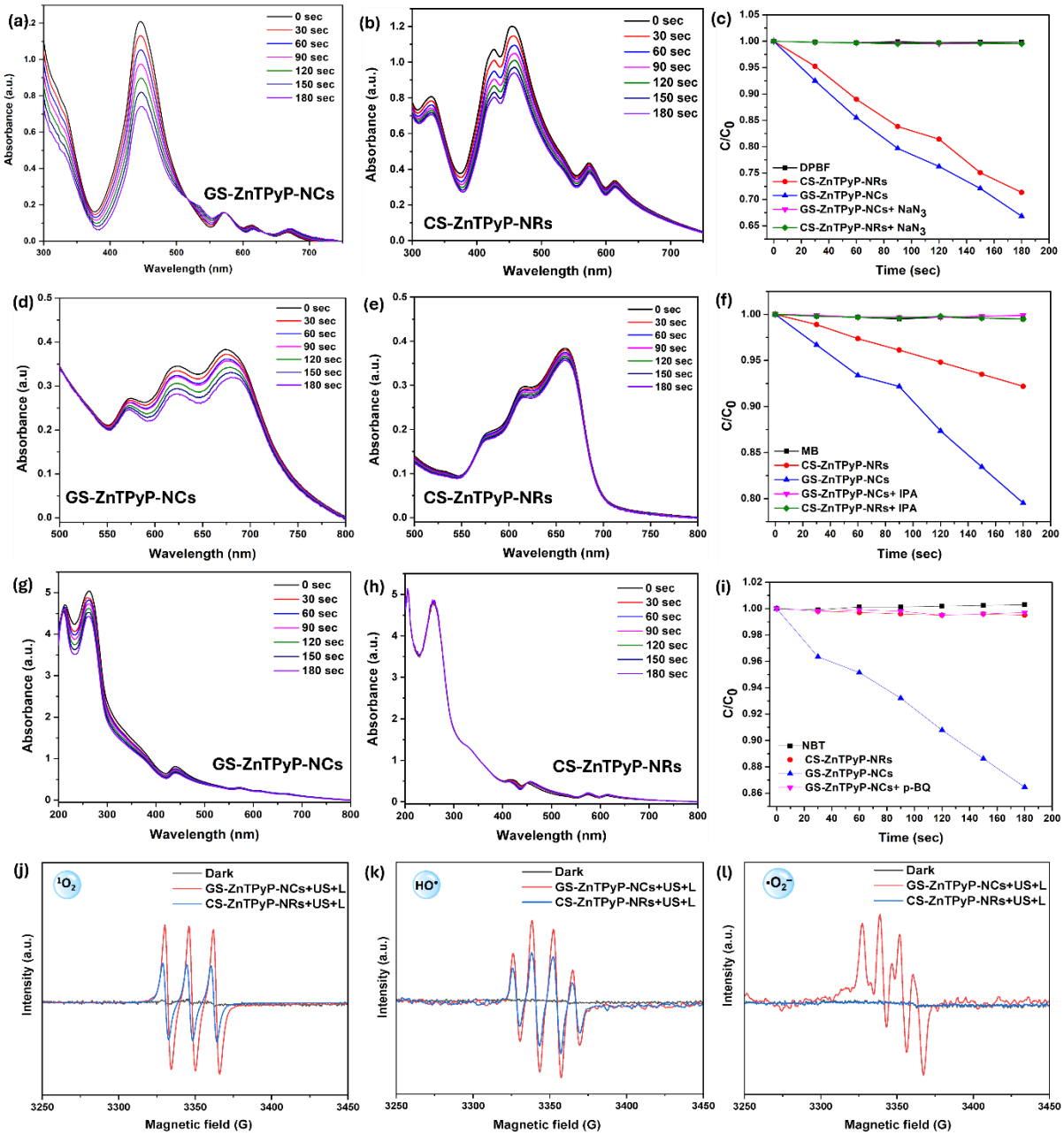

Fig. S11 ROS generation ability. (a,b) Time-dependent sono-photodegradation of DPBF indicating $^1O_2$ generated by porphyrin NPs under combined US+light irradiation. (c) The elimination ratio of DPBF. (d,e) Time-dependent sono-photodegradation of MB indicating •OH generation. (i) Elimination ratio of MB. (g,h) Time-dependent sono-photodegradation of NBT indicating $•O_2^-$ generation. (i) Elimination ratio of NBT. ESR spectra of ZnTPyP nanoparticles under combined US and light irradiation with TEMP for (j) $^1O_2$ detection. with DMPO for (k) •OH radical detection, (l) $•O_2^-$ radical detection (under different conditions).

Antibacterial Sono-photodynamic Therapy (aSPDT)

In order to determine the sono-photodynamic antibacterial efficiency of synthesized nanoparticles, Gram-negative *Escherichia coli* (*E. coli*) and Gram-positive *Staphylococcus aureus* (*S. aureus*) were selected as model organisms and the growth of bacteria under different conditions was calculated by a plate-counting method. All the glassware, culture media, and other reagents used in the experiments were pre-sterilized in the autoclave at 121 °C for 15 min. The bacterial cells were cultured in Luria–Bertani (LB) medium at 37 °C for 18 h to obtain a final bacterial density of approximately 1×10^8 CFU mL^{-1}.

E. coli and *S. aureus* were suspended in phosphate buffer saline (PBS) in a 20 mL glass vial with the concentration adjusted to about 1×10^8 CFU mL^{-1}, followed by the addition of nanoparticles, and the total volume was kept at 5 mL. The bacteria suspensions mixing with nanoparticles irradiated with US (1.0 MHz, 1.5 W cm^{-2}) and 670 nm deep-red light LEDs separately and combined for 20 min. It should be noted that the vial should be kept in the dark during the whole procedure before exposed to light and ultrasound sources. After being cultured for 2 h, the bacterial suspension was diluted 10^6 times using ultrapure water and inoculated on a solid LB agar plate. After incubation at 37 °C overnight, the CFUs were counted to evaluate the bactericidal effect of each material. Control experiments were performed using bacterial cultures without the addition of materials or irradiation to assess the inherent bacterial growth, the effects of light and ultrasound exposure alone, and the potential cytotoxicity of the materials in the absence of light and ultrasound. All antibacterial experiments were performed in triplicate. The inhibition ratios (IR) were calculated as follows-

$$\mathrm{IR}(\%) = 1 - (\mathrm{CFU}_i/\mathrm{CFU}_0) \times 100\%$$

where CFU_0 refers to CFU of bacteria cultured without materials, light, and US, while CFU_i represents the CFU of bacteria cultured under-investigated conditions.

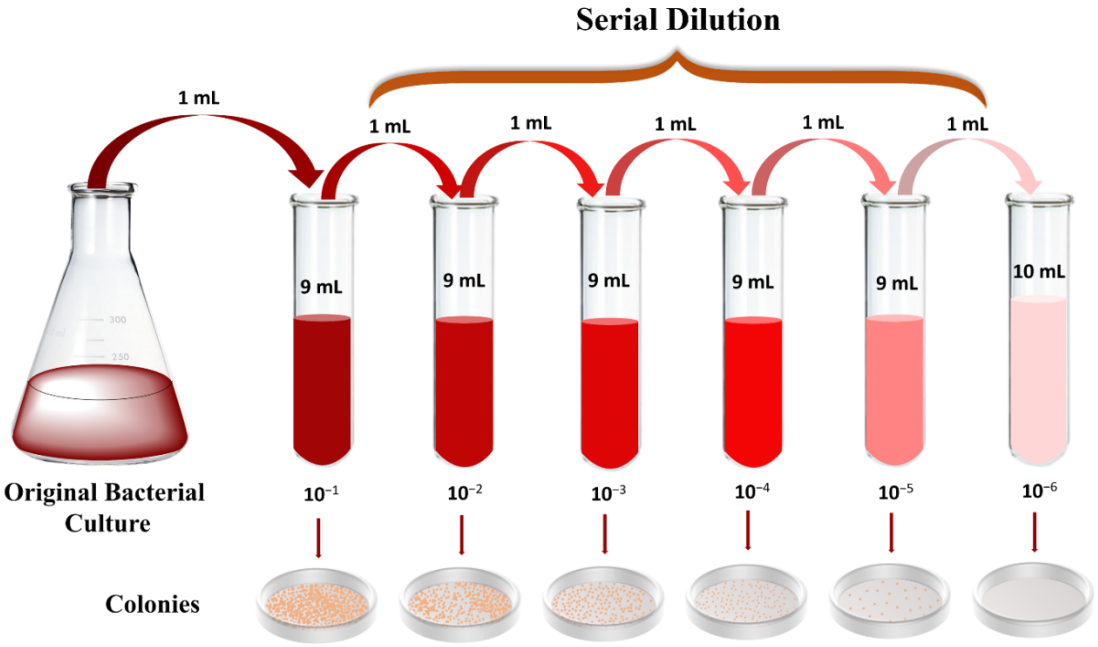

Fig. S12. General Methodology for the quantification of bacterial colonies by colony counting method.

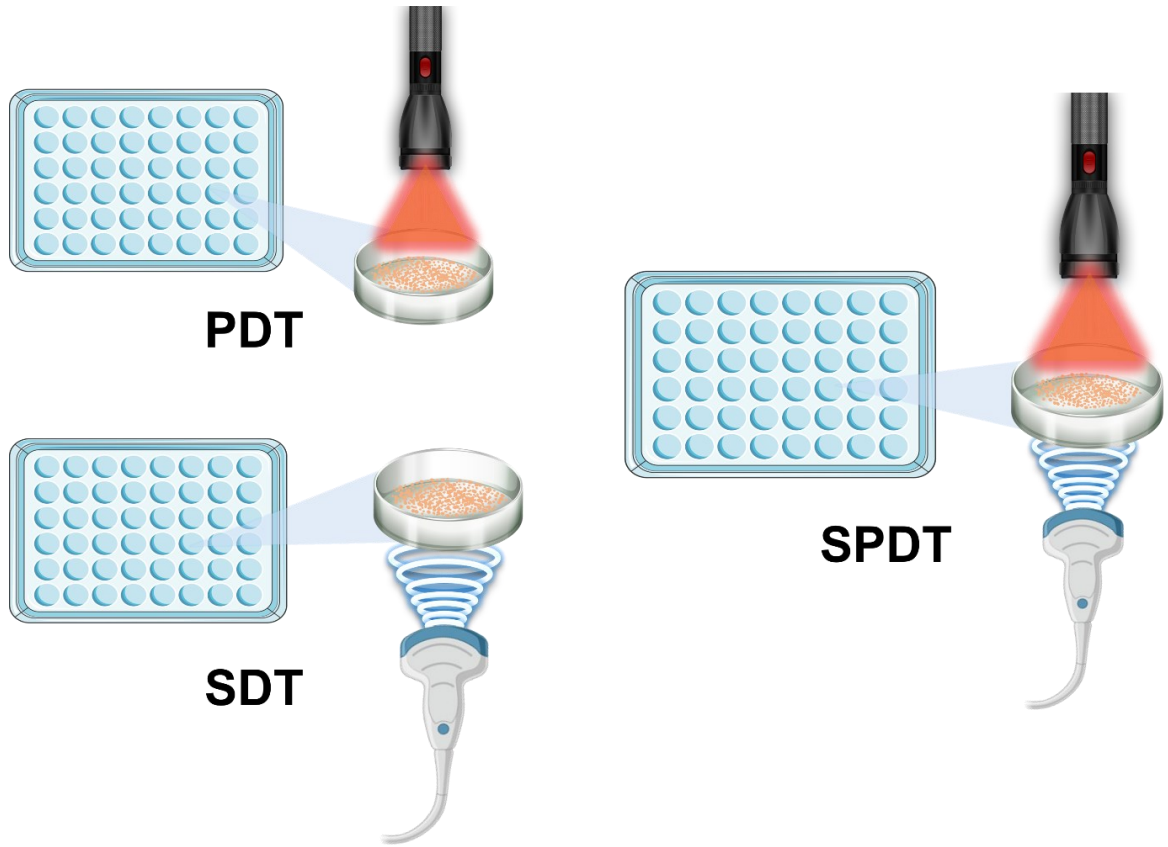

Scheme S7. Illustrative scheme of the application of light (PDT), ultrasound (SDT) and combined light and ultrasound (SPDT) for antimicrobial sono-photodynamic therapy.

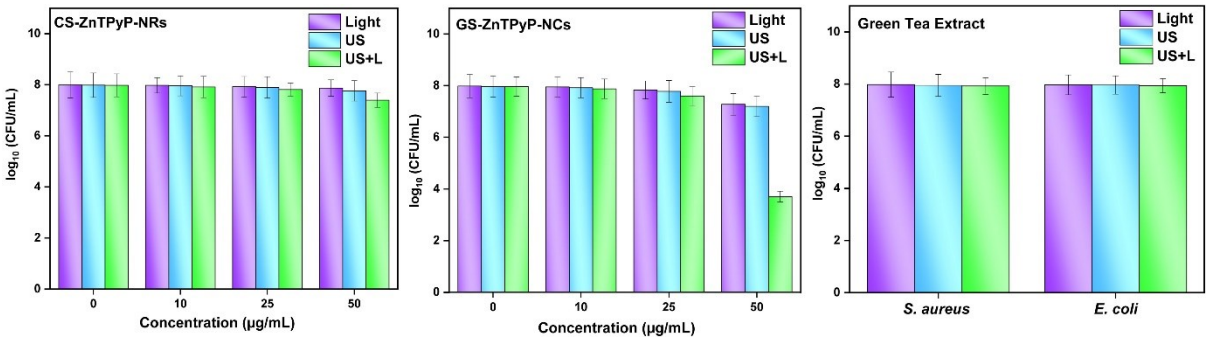

Fig. S13 Concentration dependent aPDT, aSDT and aSPDT activity of (a) CS-ZnTPyP-NRs (b) GS-ZnTPyP-NCs against *S. aureus*, (c) aSPDT activity of green tea extract (0.1 mg mL^{-1}) against *S. aureus* and *E.coli*.

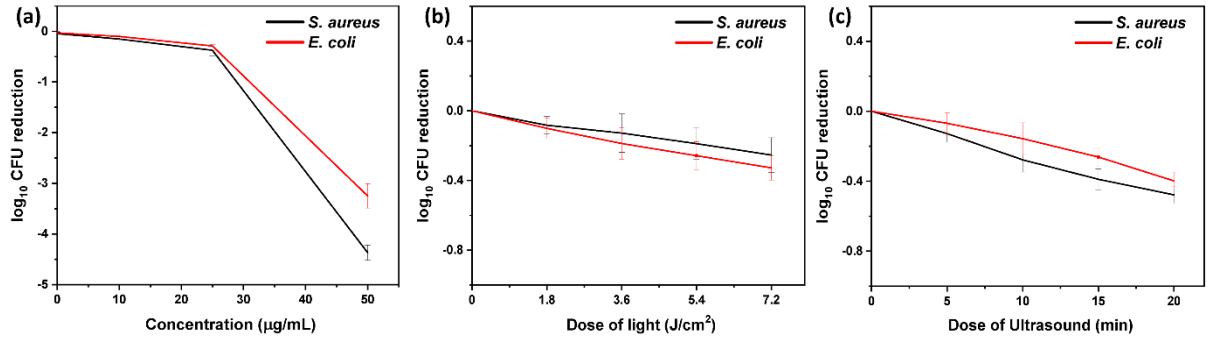

Fig. S14 Dose response curve with logs of killing, against (a) concentration of GS-ZnTPyP-NCs (μg mL^{-1}) (b) dose of light (J/cm^2), and (c) dose of ultrasound (min of irradiation) at fixed concentration of GS-ZnTPyP-NCs (50 μg mL^{-1}) for *S. aureus* and *E.coli*.

Morphological studies of Bacteria using Field-Emission Scanning Electron Microscopy

To better investigate the antimicrobial ability of the samples, the morphometric investigation of bacterial cells was evaluated using FESEM. After using by US irradiation for 10 min and then 670 nm deep-red light irradiation for 10 min, the bacteria (*S. aureus and E. coli*) were fixed with 2.5% glutaraldehyde of 2 h solution at 4 °C for overnight and washed with PBS (pH = 7.0) three times. Further, the bacteria were dehydrated with different concentrations of ethanol (30%, 50%, 70%, 90%, and 100%) for 15 min and air-dried. After being sputtered with a layer of gold according to the sample preparation method of scanning electron microscopy, the morphological changes in bacterial samples were observed with FESEM.

Plausible mechanism of sono-photoinactivation of bacteria

The plausible mechanism of sono-photoinactivation of bacteria using porphyrin involves a combination of both PDT and SDT mechanisms.[8] Upon light irradiation, porphyrin molecules are excited, and through Type I and Type II photochemical reactions, they generate ROS such as singlet oxygen ($^1O_2$) and superoxide radicals. These ROS cause oxidative damage to bacterial cell walls, proteins, and DNA, leading to bacterial death.

While the processes involved in PDT are well understood, the exact mechanisms driving SDT are still under investigation.[9] A key contributor to SDT is acoustic cavitation, where ultrasound induces the formation and oscillation of gas bubbles in the medium. These bubbles either undergo stable cavitation, oscillating and causing localized mixing effects, or inertial cavitation, where they collapse, releasing high-energy shockwaves. This collapse generates localized high temperatures and pressures, which can activate the sonosensitizer, leading to ROS production. Additionally, sonoluminescence, the emission of light due to cavitation, can further excite porphyrins and contribute to ROS generation.[10] The combination of these effects—mechanical disruption from cavitation, and enhanced ROS production through both light and ultrasound—greatly enhances the bactericidal effects of porphyrin-based sono-photodynamic therapy.

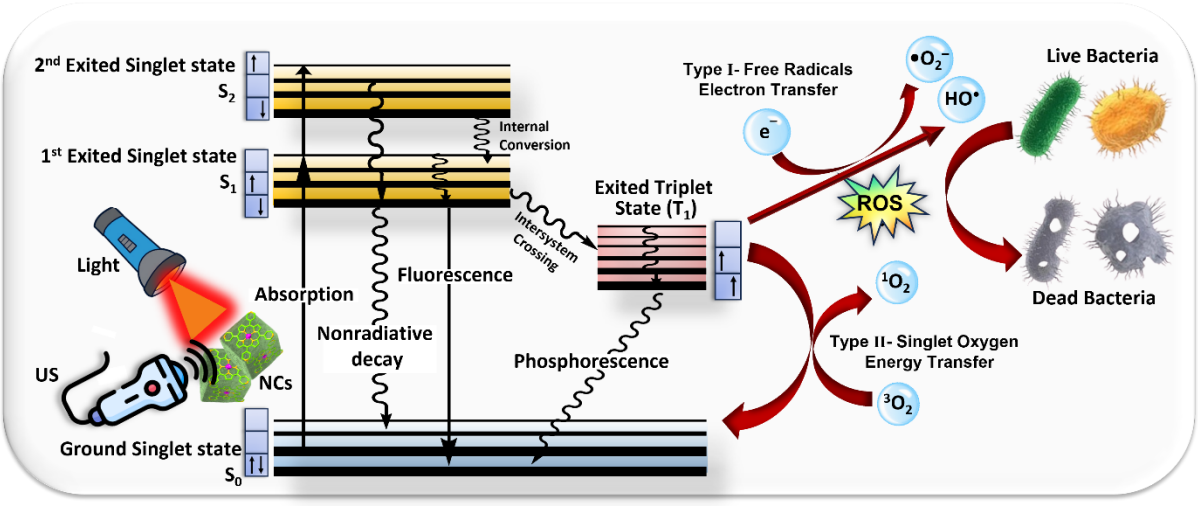

Scheme S8 Schematic diagram of the mechanism of sono-photoinactivation of bacteria.

Statistical analysis

All the results in this work are expressed as mean values ± standard deviation with $n \geq 3$. A one-way analysis of variance (ANOVA) and Student's t test were performed for significance analysis. Asterisk (*) denotes statistical significance between bars (*$p < 0.05$, **$p < 0.01$, ***$p < 0.001$) conducted using GraphPad Prism 8.0.2.

References

S1 A. D. Adler, F. R. Longo, J. D. Finarelli, J. Goldmacher, J. Assour and L. Korsakoff, *J. Org. Chem.*, 1967, **32**, 476.

S2 S. Muratsugu, A. Yamaguchi, G. I. Yokota, T. Maeno and M. Tada, *Chem. Commun.*, 2018, **54**, 4842–4845.

S3 D. Wang, L. Niu, Z. Y. Qiao, D. B. Cheng, J. Wang, Y. Zhong, F. Bai, H. Wang and H. Fan, *ACS Nano*, 2018, **12**, 3796–3803.

S4 A. K. Pujari, R. Kaur, Y. N. Reddy, S. Paul, K. Gogde and J. Bhaumik, *J. Med. Chem.*, 2024, **67**, 2004–2018.

S5 M. Michelle, M. S. J., A. J. G. and W. Gerry, *Appl. Environ. Microbiol.*, 2009, **75**, 1932–1937.

S6 A. Selim, S. Kaur, A. H. Dar, S. Sartaliya and G. Jayamurugan, *ACS Omega*, 2020, **5**, 22603–22613.

S7 J. Jiao, J. He, M. Li, J. Yang, H. Yang, X. Wang and S. Yang, *Nanoscale*, 2022, **14**, 6373–6383.

S8 F. Alves, E. T. P. Ayala and S. Pratavieira, *J. Photochem. Photobiol.*, 2021, **7**, 100039.

S9 F. Giuntini, F. Foglietta, A. M. Marucco, A. Troia, N. V. Dezhkunov, A. Pozzoli, G. Durando, I. Fenoglio, L. Serpe and R. Canaparo, *Free Radic. Biol. Med.*, 2018, **121**, 190–201.

S10 R. Canaparo, F. Foglietta, N. Barbero and L. Serpe, *Adv. Drug Deliv. Rev.*, 2022, **189**, 114495.